Paleomagnetic data place the Burma Terrane in a Trans-Tethyan arc colliding with India (Supplementary Information)

1. Geological summary

1.1. Myanmar

The present-day tectonic setting of Myanmar is characterized by active hyper-oblique subduction of Indian crust beneath the Burmese margin [1–3]. Within this setting, two broadly north–south oriented major blocks are often distinguished: The Burma Terrane (BT), and the Shan Plateau on the Sibumasu Block (Fig. 2). The BT has been called West Burma Block before, but we prefer the name Burma Terrane, because its tectonic history is significantly different from surrounding features as explained below. The collision age of the BT with the Sibumasu Block is not well constrained and even the existence of a suture between both blocks is challenged [4,5]. The western border of the Sibumasu Block presents a complex belt of metamorphic rocks, called the Mogok–Mandalay–Mergui Belt (MMMB) which records two main metamorphic events: A late Cretaceous – early Paleocene phase of metamorphism and partial melting, followed by a phase of late Eocene - Oligocene high-temperature metamorphism [6]. Certain areas of Shan Scarps in the MMMB have been interpreted as a shear zone, either as part of a dextral or sinistral tectonic regime [7–9]. In any case, major dextral displacements between the BT and the Sibumasu Block have occurred since the late Miocene along the active Sagaing Fault, which forms the present-day tectonic boundary between the two blocks. These displacements have been estimated up to 400 km [1,2,10–12]. Other examples of dextral strike-slip faults in eastern Myanmar are the Neogene South Sagaing Fault and the late Oligocene West Andaman Fault to the south [13]. The Jade Belt ophiolite [6,14,15] is found at the northern end of the Sagaing fault and is part of the BT. Oceanic crust of ~163 Ma is incorporated in this ophiolite, while the jadeite itself has varying age constraints [6,16].

The western boundary of the BT is delineated by the Kabaw Fault or the ~127 Ma Western Belt Ophiolite in the Indo-Burman Ranges (IBR) [6,14,17,18]. The most recent detrital zircon studies of the Late Triassic Pane Chaung Formation, a key turbiditic sedimentary sequence directly flanking the Western Belt ophiolites in the IBR [19–21], indicate either a late Mesozoic Gondwana or Cathaysian origin for this formation [20,21]. The subduction of Neo-Tethyan oceanic crust marked the beginning of the development of the present-day Andean-type Burmese subduction margin, leading to the development of multiple N-S trending Cretaceous-Neogene forearc and back-arc basins on the BT which are collectively called the Central Myanmar Basins. The forearc and back-arc are separated by the N-S trending Cretaceous-Neogene Wuntho-Popa Arc, an Andean-type volcanic arc, as evidenced by the occurrence of I-type batholiths and andesitic bodies [22–24]. Published U-Pb data suggest a main magmatic event from 110-90 Ma, followed by subordinate stage from 70-30 Ma [14,24–26]. The Western Belt Ophiolite was likely emplaced during the Late Cretaceous as well [23,24,27–29].

The focus of this study is on two areas on the BT: The Wuntho Range and the Chindwin Forearc Basin (Fig. S1) [19,30].

1.2. Chindwin Basin

The paleomagnetic sampling in the Chindwin Basin was made near the town of Kalewa, western Myanmar (Fig. S1). Below is a brief summary of the geology of the Chindwin basin described by a previous study [28]. The Chindwin Basin is the northernmost forearc sub-basin of the Central Myanmar Basins, situated on the BT. On its western side, the basin infill is deposited on top of the Western Belt ophiolites. To the east, the basin is delineated by the Wuntho-Popa Arc. The sedimentary sequence is homoclinal around Kalewa, and starts with Albian-Eocene marine deposits, followed by the westward-directed fossil-rich fluvio-deltaic sediments of the late middle Eocene Pondaung Formation. The overlying upper Eocene Yaw Formation is characterized by both shallow marine and lacustrine continental intervals, indicating a quasi-closed estuarian depositional environment. Sandstones and mudstones are the dominant sediments in the Yaw Formation (Fig. S2e). They are

intercalated with coal- or gastropod- bearing layers, as well as early-diagenetic siderite-rich carbonate layers (Fig. S2f). Siderite is often one of the earliest minerals to precipitate in sediments and is formed during shallow burial as a result of bacterial reduction in anoxic or suboxic conditions [31]. A single tuff layer is also present in the Yaw Formation, yielding an age constraint of ~38 Ma [28]. The Yaw Formation is overlain by an Oligocene - Pliocene continental fluvial sequence consisting of the Letkat, Natma, Shwetamin and Irrawaddy Formations, marking the uplift of the IBR in the west. The Paleocene – Eocene sediments are mostly derived from the Wuntho-Popa Arc, while erosion of metamorphic rocks, from the MMMB and the IBR, also contributed to the Oligocene - Miocene basin fill [28].

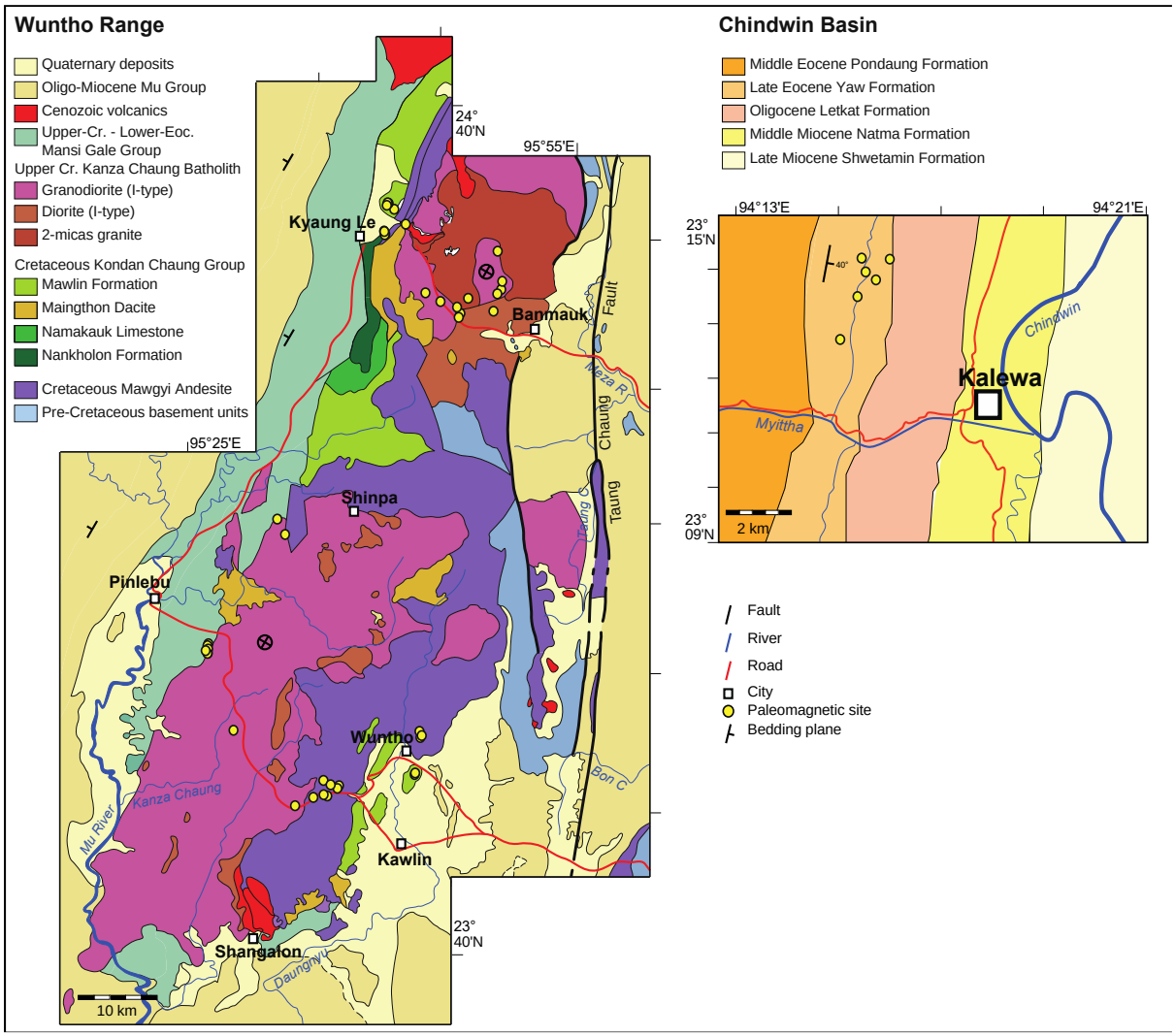

Figure S1: *Geological maps of study areas: Wuntho Range (Left), Kalewa, Chindwin Basin (Right)* [19,30].

Figure S2: *Representative outcrops and lithologies from this study. Site name, lithology and locality are indicated per image.*

1.3. Wuntho Arc

The Wuntho Range is located in the northern BT (Fig. S1). It is the northern segment of the Upper Cretaceous to Eocene Wuntho-Popa Arc that subdivides the Central Myanmar Basins into forearc and back-arc basins. Its main component is the early Late Cretaceous Kanza Chaung Batholith. The arc has been correlated either with the Gangdese Arc or with the Indonesian Woyla Arc, based on similarities in age and lithology [4,17]. Despite limited outcrops exposure in the Wuntho Range, fresh outcrops were found in rivers as well as quarries used for road construction. Apart from our own observations, the descriptions of Wuntho Range lithologies are mostly taken from detailed United Nations geological reports [19] that have been recently updated in a special volume on Myanmar geology [30]. The Hpyu Taung Metamorphics, the Ubye Serpentinite Complex and the Shwedaung Formation constitute the basement rocks of the Wuntho Range and are part of the BT. The Hpyu Taung Metamorphics consists of high-grade metamorphic rocks and granites, while the Shwedaung Formation is a low-grade metamorphic sequence of sediments, extrusives and volcaniclastics. The contact with younger lithologies in the area is uncertain, but the age of the Shwedaung Formation is believed to be Late Triassic based on similarities with the Pane Chaung Formation in the IBR, western Myanmar. A sequence of Cretaceous volcanics and sediments lies unconformably on top of these basement rocks (Fig. S2a,c,d). The Mawgyi Andesite is poorly dated, but has been interpreted as the oldest formation of this Cretaceous sequence. These volcanics are the most extensive extrusives in the area. They are typically massive, with a grey to green or black colour, alternating with finer brecciated flows and agglomerates, as well as occasionally volcanogenic sediments. Sills and dikes can be found intruding the other lithologies. Previous studies have suggested that the Mawgyi Andesites are a remnant of an oceanic arc thrusted on the BT prior to the establishment of the Wuntho-Popa Arc [4,17]. However, we do not observe field evidence for a major thrusting event in the Wuntho Range. Moreover, our $^{40}Ar/^{39}Ar$ dating of the Mawgyi Andesite yields an age contemporaneous with the Kanza Chaung batholith (Supplementary section 3), suggesting that they were emplaced contemporaneously or during a precursory extrusive phase. The Kondan Chaung

Group comes after the Mawgyi Andesite in the Wuntho Range stratigraphy. This sequence has a diverse composition, consisting of sandstones, limestones, volcaniclastics and (rhyo-)dacites. It is predominantly exposed in the northern part of the Wuntho Range. The Maingthon Dacites are the minor volcanic part of the Kondan Chaung Group. These dacites are generally porphyritic with a bleached white to dark grey-green colour. It also contains massive rhyodacite flows with a grey-purple colour with few phenocrysts. The presence of pyrite, sulphide and chlorite suggests hydrothermal alteration. The sandstones and siltstones of the Mawlin Formation are also part of the Kondan Chaung Group. They typically have a grey-brown to greenish colour. Fining-upwards sequences and cross-bedding are common sedimentary structures in this formation, corresponding to a turbiditic facies. Locally, tuffaceous deposits and breccia layers are mixed or interbedded with these sediments. The overlying limestones of the Namakauk Formation contain shell debris and abundant algae together with volcanic fragments, but lack age-diagnostic fossils. The Kondan Chaung Group underwent a significant amount of folding. On the other hand, the Kanza Chaung Batholith (Fig. S2b) shows no signs of significant tilting. This NE-SW trending batholith constitutes the main component of the Wuntho Range, exposed in a large part of the area. The batholith primarily consists of medium to coarse I-type (grano)diorites with several mafic inclusions, as well as smaller diorite plutons and an area consisting of 2-mica granite in the north. U-Pb dating of these intrusions yielded ages of ~100 Ma [25,30]. A second phase of I-type magmatism of late Eocene age is found at the Shangalon copper district[30]. A Late Cretaceous – Paleogene sequence of sediments, postdating the main Kanza Chaung Batholith, surrounds the Wuntho Range, resulting in an apparent regional NE-SW trending anticline. In the west, the thick stratigraphic succession of predominantly sedimentary rocks dip to the northwest to form the eastern limb of the Chindwin Basin. There is no major known thrust between the Chindwin Basin and the Wuntho Range. To the east of the Wuntho Range, the sedimentary basins are disrupted by major faults (Taung Chaung Fault) and deformation related to displacements along the Sagaing Fault system.

2. Petrology

Because of the complex character of Wuntho Range geology and for a better understanding of the paleomagnetic record, petrological analysis was conducted on several samples with both an optical microscope and a Scanning Electron Microscope (SEM). Relevant observations resulting from this analysis are shown below per locality.

2.1. Kanza Chaung Batholith

The majority of samples from the Kanza Chaung Batholith are (grano)diorites. This is clearly confirmed by microscope observations under both transmitted and cross-polarized light, in a sample from site MY04, Pinlebu. We observe no alteration in accordance with previous studies [19,25,30].

2.2. Mawgyi Andesite

Optical microscope images of andesitic samples from sites MY08, MY10 and MY11 all exhibit signs of alteration (Fig. S3a-d). In MY08, larger plagioclase grains exhibit altered rims under the optical microscope, which could correspond to either low-grade metamorphism or hydrothermal alteration (Fig. S3a). In MY10, brecciation is suggested by the juxtaposition of crystal-rich parts and aphanitic ones (Fig. S3b-c), with the latter parts containing large vacuoles and chlorite-epidote metamorphism (Fig. S3b). Both MY08 and MY10 contain large calcite veins, as evidenced by SEM analysis (Fig. S3c-e). In fact, calcite is not only observed in veins, but is also partly penetrating the sample matrices. On the other hand, in site MY11, quartz alteration is observed instead of calcite alteration. Chalcopyrite was only observed in some samples (MY10, Fig. S3h). A large amount of magnetite is observed in most samples with various grain size (Fig. S3e-h). The largest magnetite grains often contain titanite inclusions. The micron-size magnetite grains are found in close association with calcite alteration (Fig. S3e). All these observations point towards the presence of either calcite or quartz hydrothermal alteration due to local mineralizing events, as well as low-grade chlorite-epidote metamorphism in the Mawgyi Andesite.

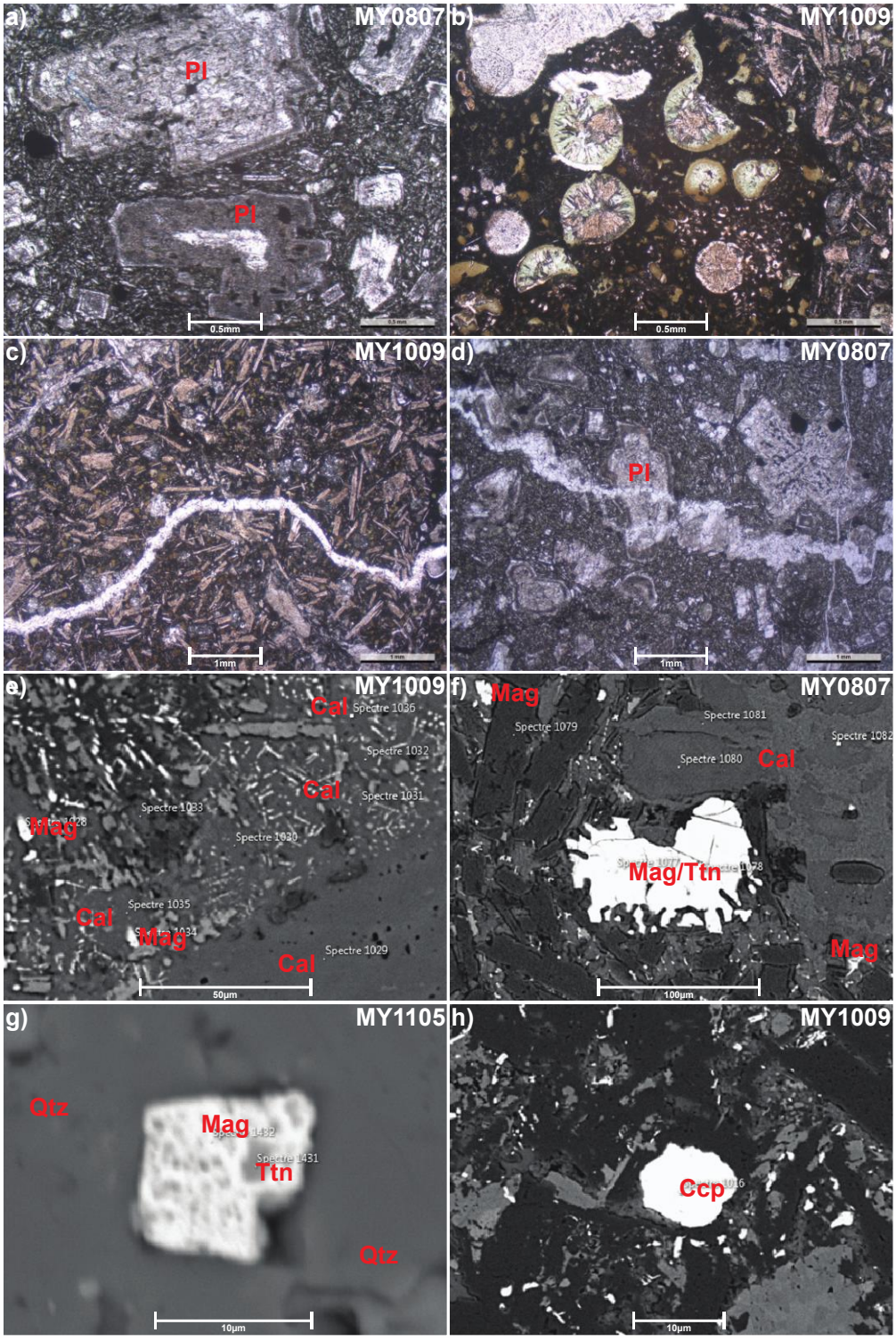

Figure S3: *Representative microscope images from the Mawgyi Andesite, Wuntho Range. Sample name and scale are indicated per image. Mineral abbreviations (red): Cal = calcite, Ccp = chalcopyrite, Mag = magnetite, Pl = plagioclase, Qtz = quartz, Ttn = Titanite.*

2.3. Kondan Chaung Group

The Kondan Chaung Group is the most variable in lithology, containing sandstones, limestones, volcanic and volcaniclastic lithologies. They all display various types of alteration according to the lithology (Fig. S4). Site MY22, a very fine-grained volcanic sill or dike, contains large iron-oxide grains (Fig. S4a) with pervasive titanite alteration. Titanite is found especially replacing previous lamellae formed by primary exsolution of titanomagnetite to ilmenite or ulvöspinel. This process is indicative of posterior hydrothermal alteration [32].

MY45 is a mixture of siltstone and pyroclastic material, containing large unaltered quartz grains. However, the glass and silicate matrix have been replaced with secondary quartz and calcite (Fig. S4d). Site MY25 is another volcanic sandstone and fine breccia. Quartz recrystallization is important in this site and secondary crystallization of Ti-oxides indicates dissolution of previous detrital Ti-Fe oxides. The same observation is made for the sandstones from site MY24 and MY41. The most striking feature in these sedimentary rocks is the widespread authigenic formation of small TiO_2 oxides with in some cases sub-micron zircons in close association with the titanium oxides (Fig. S4c). Iron-oxides in the form of magnetite or hematite were not recognized in SEM.

The fossil-rich limestone at site MY23 contains framboidal pyrite (Fig. S4b). SEM data shows altered silicate clast assemblages (Fig. S4e,f) with likely relict lattice of micron-size Ti-oxide and apatite rods after dissolution of magnetite.

Kondaung Chaung sandstones were also drilled at site MY34, near Kawlin. The lithology is different from the sandstones at sites MY24 and MY41. At Kawlin, volcanic clasts and silicate minerals are less pervasively replaced. This is the single site where we identify detrital chalcopyrite grains (Fig. S4g), suggesting that the sandstones are derived from the nearby mineralized Mawgyi Andesite. Secondary iron-sulphurs, mainly pyrite, are found in veins and fractures (Fig. S4h). In contrast with the sites near Kyaung Le, titanite is present instead of secondary TiO_2 minerals.

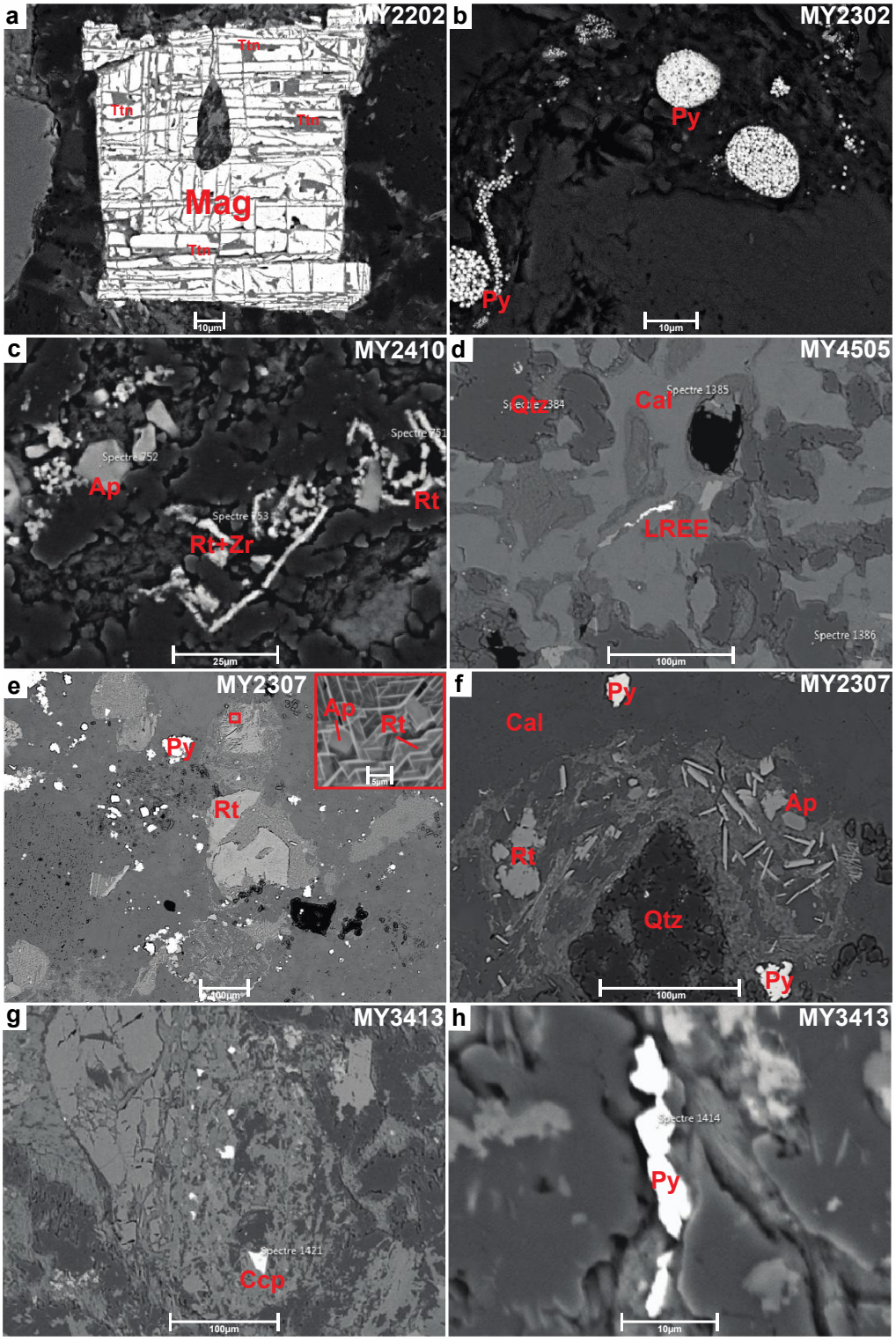

Figure S4: *Representative microscope images from the Kondan Chaung sediments, Wuntho Range. Sample name and scale are indicated per image. Mineral abbreviations (red): Ap = apatite, Cal = calcite, Ccp = chalcopyrite, LREE = Light Rare Earth Elements, Mag = magnetite, Py = pyrite, Qtz = quartz, Rt = Rutile, Ttn = Titanite, Zr = Zircon.*

3. $^{40}Ar/^{39}Ar$ dating

From the total of 14 measured samples, nine yielded interpretable $^{40}Ar/^{39}Ar$ plateau dates on whole rock samples, as well as amphiboles and biotites (Fig. S5, Supplementary Data 3). $^{40}Ar/^{39}Ar$ dates from the batholith range from ~97 to ~87 Ma and are only slightly younger than reported U-Pb dates (~103-97 Ma) [14,25,26].

Age determination of the Mawgyi Andesite was no possible due to the low potassium content. A minimum date of 100.9±0.2 was obtained in site MY07, indicating that at least part of the Mawgyi Andesite is younger than the previously interpreted Early Cretaceous age, although it could also be reset by low-grade metamorphism during batholith emplacement.

At Kyaung Le, the two plateau dates obtained at site MY22 and MY43 confirm that these rocks are contemporaneous with the batholith emplacement.

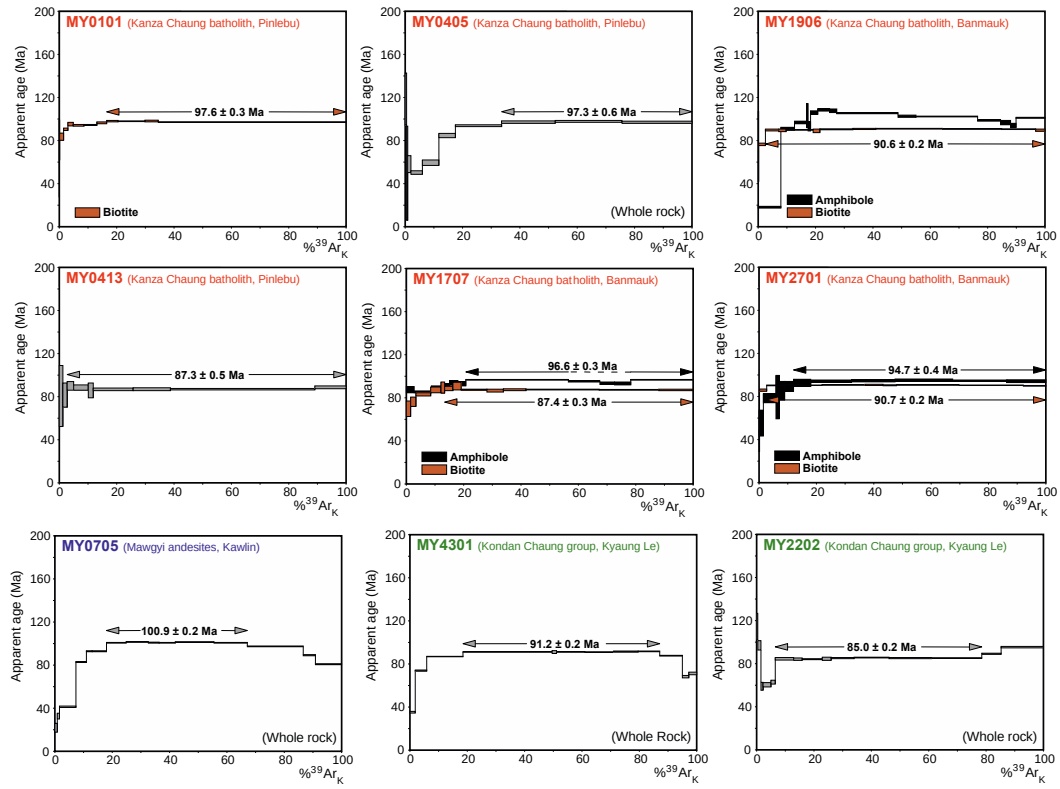

Figure S5: *$^{40}Ar/^{39}Ar$ dates for representative sampled sites in the Wuntho arc.*

4. Paleomagnetic results

The results are presented according to the location and the distinct sampled rock types, which control the magnetic behaviour in demagnetization. Both progressive thermal demagnetization with steps of 30 to 50°C and AF demagnetization were used to identify the characteristic remanent magnetization (ChRM). The resulting mean directions are given per site and locality in Supplementary Data 1, while all resulting directions from each paleomagnetic sample are listed in Supplementary Data 2.

4.1. Pinlebu, Shinpa & Banmauk (Kanza Chaung Batholith)

The whole rock magnetic properties (magnetic susceptibility, coercive fields, Curie points) are mainly controlled by multidomain magnetite. For six out of eleven sampled sites near Banmauk, the intensity of the natural remanent magnetization (NRM) is usually very low ($< 2\ 10^{-2}$ Am^{-1}) after 10 mT and no well-defined ChRM was recovered. At the other sites however, a small amount of fine-grained magnetite was sufficient to record interpretable ChRMs, which were recovered by AF above 15-20 mT or thermal demagnetization above 400°C (Fig. S6a). Reliable paleomagnetic results were obtained at four sites around Pinlebu area, at three sites around Shinpa and at five sites around Banmauk (Fig. S6c, Supplementary Data 1). The Pinlebu and Shinpa sites give well-determined paleomagnetic means with an east oriented declination and nearly horizontal inclination. The ChRM directions from Banmauk yield east-oriented declinations as in Pinlebu, but with a slightly negative inclination and a larger scatter in declination. Unrecognized small tilts or local-block rotations may contribute to this scatter. There is no field evidence for significant wholesale tilting of the complete batholith.

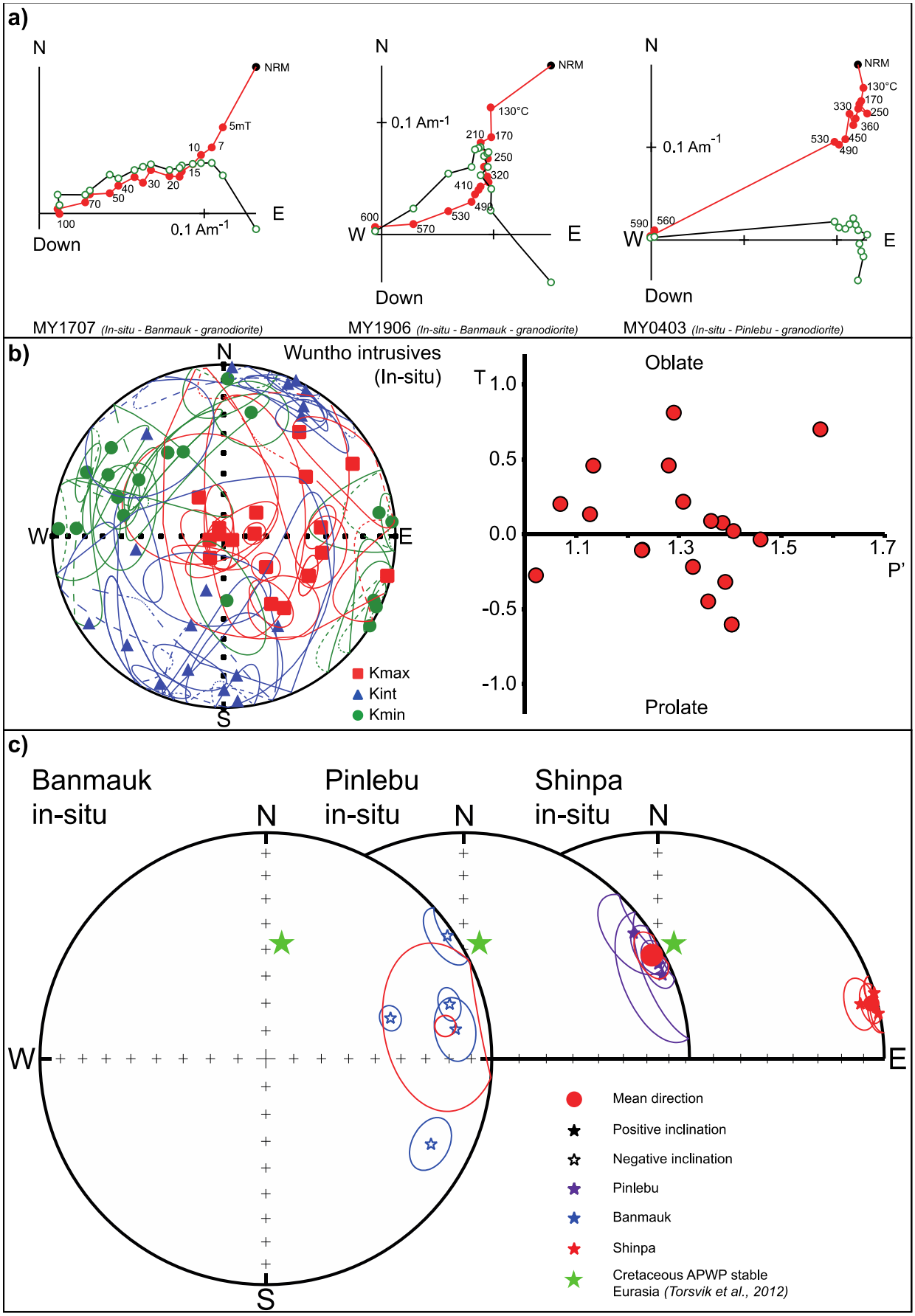
a)
N
NRM
5mT
10
7
15
40
30
20
50
70
100
E
0.1 Am-1
Down
MY1707 (In-situ - Banmauk - granodiorite)
0.1 Am-1
130°C
210
170
250
320
410
490
530
600
570
W
MY1906 (In-situ - Banmauk - granodiorite)
330
250
360
530
450
490
590
560
MY0403 (In-situ - Pinlebu - granodiorite)
b)
Wuntho intrusives
(In-situ)
Kmax
Kint
Kmin
Oblate
Prolate
T
P'
1.0
0.5
0.0
-0.5
-1.0
1.1
1.3
1.5
1.7
c)
Banmauk
in-situ
Pinlebu
in-situ
Shinpa
in-situ
Mean direction
Positive inclination
Negative inclination
Pinlebu
Banmauk
Shinpa
Cretaceous APWP stable
Eurasia (Torsvik et al., 2012)

Figure S6: *Paleomagnetic results from the Kanza Chaung Batholith, Pinlebu, Shinpa and Banmauk, Wuntho Ranges: a) Representative orthogonal demagnetization plots. Open/closed dots denote projections on the vertical/horizontal plane. Reference frame, locality and lithology are indicated per plot; b) left) Equal-area projection of mean-site anisotropy of magnetic susceptibility (AMS) results with ellipse of confidence at 95%; right) Plot of the shape of the anisotropy ellipsoid (T) versus the corrected anisotropy degree; c) Equal-area projection of the mean-site characteristic directions of all reliable paleomagnetic data in in-situ coordinates.*

The anisotropy of magnetic susceptibility (AMS) results from the Wuntho intrusions have a generally sub-vertical NE-SW trending magnetic foliation with a near vertical lineation (Fig. S6b). This means that AMS foliations of the Kanza Chaung Batholith are roughly parallel to the general trend of the Wuntho Arc, further indicating that the batholith was not tilted. The degree of AMS P' is high (~1.1-1.4 for most samples, Fig. S6b), but mainly controlled by multidomain magnetite. In order to test the effect of anisotropy on the ChRM, we obtained anisotropy of remanent magnetization data. Full anisotropy of isothermal remanent magnetization (AIRM) tensors have similar fabrics than the AMS but the shape and anisotropy degree is usually higher. Because the ChRM is carried by magnetite with coercivities above 20 mT, tensors of AIRM left above 20 mT AF demagnetization (AIRM@20mT) were also calculated. The orientation of AIRM@20mT tensors is often different from the AIRM and AMS tensors, with greater scatter and an anisotropy degree below 1.5. Applying the inverse tensor to correct the ChRMs indicates that the ChRMs were not deflected by anisotropy from the original field. Therefore, anisotropy cannot account for the large tectonic rotation or latitudinal translation recorded by the intrusions.

4.2. Kawlin (Mawgyi Andesite)

High magnetic susceptibilities (> 0.01 SI in most samples) and bulk magnetic susceptibility versus temperature (K-T) experiments confirm that magnetite is the main magnetic mineral in the Mawgyi Andesite (Fig. S7c). K-T curves show slight maghemitization in some samples.

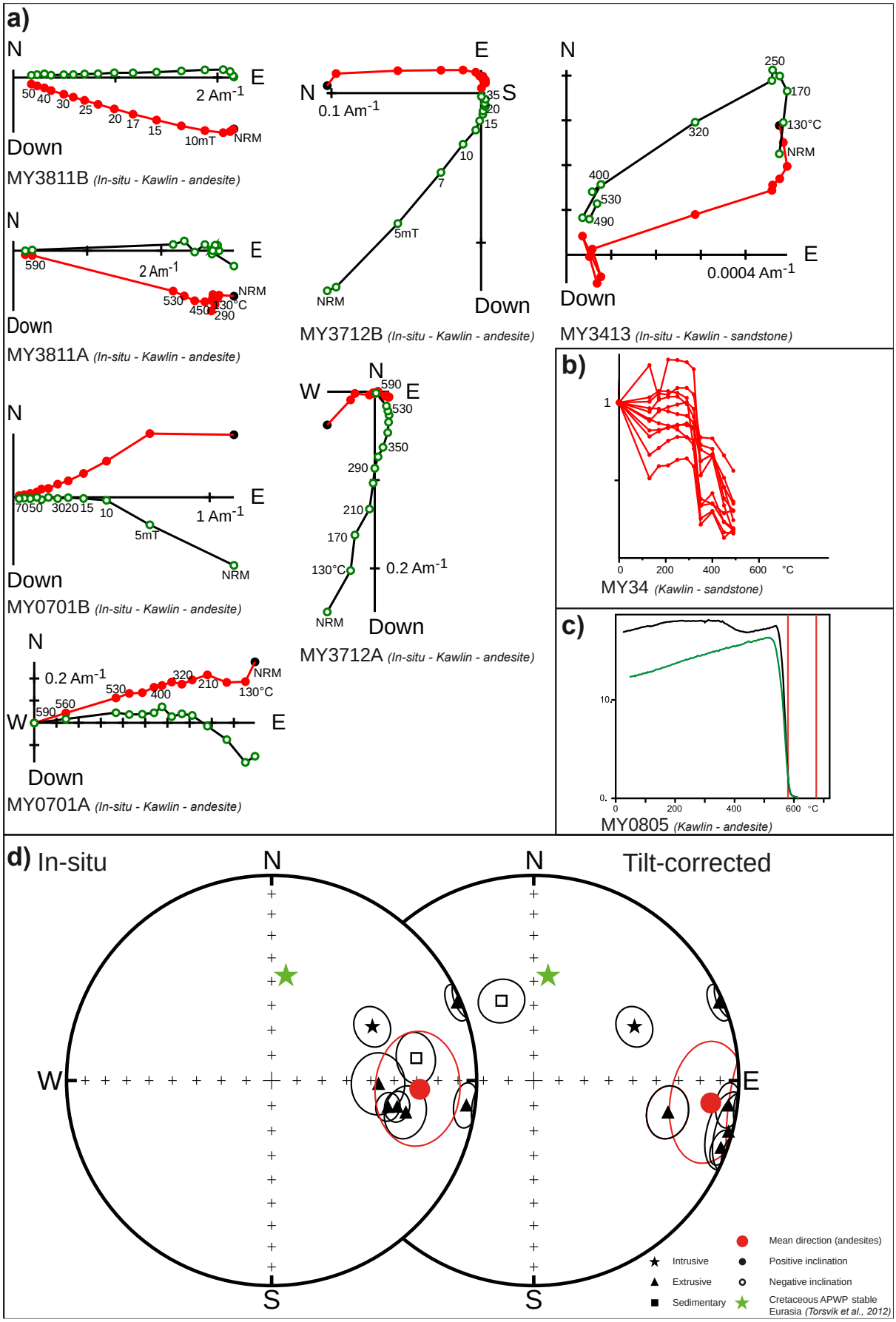
a)
N
E
2 Am-1
50 40 30 25 20 17 15 10mT NRM
Down
MY3811B (In-situ - Kawlin - andesite)
N
E
590
2 Am-1
NRM
530 450 130°C 290
Down
MY3811A (In-situ - Kawlin - andesite)
N
E
7050 3020 15 10 5mT
1 Am-1
NRM
Down
MY0701B (In-situ - Kawlin - andesite)
N
0.2 Am-1
320 210 NRM 130°C
530 400
590 560
W
E
Down
MY0701A (In-situ - Kawlin - andesite)
E
N
S
0.1 Am-1
35 20 15 10 7 5mT
NRM
Down
MY3712B (In-situ - Kawlin - andesite)
N
W
E
590 530 350 290 210 170 130°C
0.2 Am-1
NRM
Down
MY3712A (In-situ - Kawlin - andesite)
N
250 170 130°C NRM 320 400 530 490
E
0.0004 Am-1
Down
MY3413 (In-situ - Kawlin - sandstone)
b)
1
0 200 400 600 °C
MY34 (Kawlin - sandstone)
c)
10
0
0 200 400 600 °C
MY0805 (Kawlin - andesite)
d) In-situ
N
W
E
S
Tilt-corrected
N
E
S
Mean direction (andesites)
Intrusive
Positive inclination
Extrusive
Negative inclination
Sedimentary
Cretaceous APWP stable Eurasia (Torsvik et al., 2012)

Figure S7: *Paleomagnetic results from the Mawgyi Andesite, Kawlin, Wuntho Range: a) Representative orthogonal demagnetization plots from the different sampled lithologies. Open/closed dots denote projections on the vertical/horizontal plane. Reference frame, locality and lithology are indicated per plot; b) Normalized intensity of the remanent magnetization versus temperature during thermal demagnetization for all samples from sandstone site MY34; c) Variation of the bulk magnetic susceptibility (10^{-6} m^3/kg) versus temperature (°C) (K-T plot) for a representative sample of the Mawgyi Andesite showing magnetite as the main magnetic mineral. Black/ green curves are respectively the heating/ cooling curves; d) Equal-area projections of the site-mean directions of all reliable paleomagnetic data in both in-situ and tilt-corrected.*

The same ChRM was recovered after thermal demagnetization above 400-500°C and after AF demagnetization above 20 to 30 mT, in agreement with magnetite being the main magnetic carrier (Fig. S7a). The low temperature and low coercivity secondary magnetizations are often parallel to the present-day field. When the overprint is large, great circles were determined and combined with best-fit line vectors to determine the mean-site direction. Paleomagnetic results were obtained at six sites out of nine sampled sites (Fig. S7d). Two sites (MY06 and MY35) are in brecciated rocks that yield scattered paleomagnetic data despite similar magnetic properties. This observation indicates that there is no homogeneous widespread remagnetization in these rocks, despite petrologic evidence for local mineralizing events causing hydrothermal alteration at several sites. Moreover, an estimate of age (Supplementary section 3) as well as bedding from paleohorizontals flow contacts in the Mawgyi Andesites is not straightforward. The AMS degree is low (P' = ~1.0-1.1) and the magnetic fabric is either coherent or scattered at the site level. There is no clear trend in the AMS ellipsoids between sites. These complications make it difficult to provide a reliable mean direction from the andesitic sites around Kawlin, although the east oriented declination of the ChRM is similar to Pinlebu, Shinpa and Banmauk.

In addition to the andesites, two sites were drilled in the sandstones from the Mawlin Formation (MY09, MY34) south of the town of Wuntho. At site MY34, the ChRM is especially well-defined over a very limited temperature range (290-350°C) (Fig. S7a,b). Magnetite is the main magnetic remanence carrier seen in high-field experiments, but an inflection is also seen at ~300°C upon thermal demagnetization of the highest coercivity part of the IRM. Hence, we associate the sharp laboratory unblocking temperature range of the NRM with pyrrhotite and interpret the ChRM to be secondary. The sandstones are intruded by thin sills or dykes, likely related to the Kanza Chaung Batholith, suggesting that pyrrhotite was likely formed by metamorphism related to volcanic intrusion. Indeed, the application of a tilt correction results in an unrealistic, steep negative inclination for MY34. Therefore, the in-situ mean direction obtained at MY34 probably best represents the expected field direction at ~100 Ma around Kawlin (Fig. S7d, Supplementary Data 1).

A few kilometres farther west of the andesite exposures, we sampled one site in an igneous stock (MY12). This is the only site in igneous rocks where hematite is the main carrier of the ChRM. This observation might be an indication that this stock is related to the Mawgyi volcanic rocks and not to the magnetite-rich rocks of the Kanza Chaung Batholith.

4.3. Kyaung Le (Kondan Chaung Group)

4.3.1 Volcanic and volcaniclastic rocks

Samples from site MY22 have the highest intensity of magnetization (0.2-0.4 Am^{-1}) and discrete laboratory unblocking temperatures (530-580°C). The titanite replacement of titanomagnetite observed in SEM inspection (Supplementary section 2.3) demonstrates major mineralogic alteration after emplacement. The ChRM was likely acquired during this phase of alteration.

Samples from rhyodacite site MY43 have NRM intensities in the range (0.01-0.04 Am^{-1}) and magnetic susceptibilities ~0.0002 SI. Magnetite and hematite carry the same ChRM vector with respectively ~90% and ~10% of the magnetization, mostly determined above 400°C (Fig. S8a). Hematite is well-defined in IRM acquisition curves.

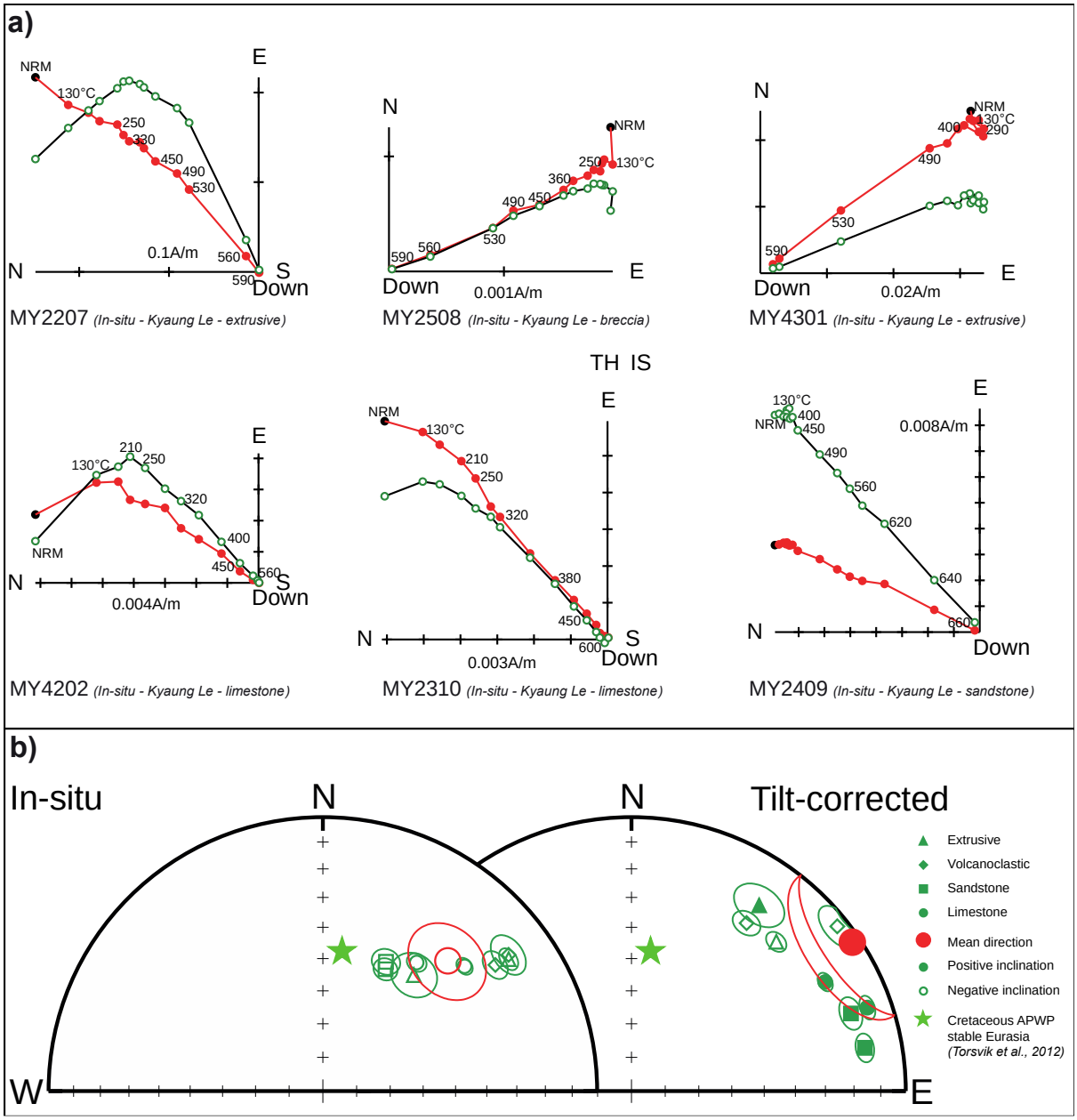

Figure S8: *Paleomagnetic results from the Kondan Chaung Group, Kyaung Le, Wuntho Range: a) Representative orthogonal demagnetization plots from the different sampled lithologies. Open/closed dots denote projections on the vertical/horizontal plane. Reference frame, locality and lithology are indicated per plot; b) Equal-area projection of the site-mean directions of all reliable paleomagnetic data in both in-situ and tilt-corrected.*

Site MY45 is in a fine-grained sedimentary rock with lenses of coarse-grained volcaniclastic rocks. Both the NRM intensity and magnetic susceptibility are low in these rocks. Site MY25 is another

coarse volcaniclastic sandstone with clasts up to a few millimeters in some samples. Samples with or without clasts both have a ChRM defined in the laboratory unblocking temperature range 400-590°C, with magnetite as the magnetization carrier (Fig. S8a). There is no evidence of hematite at these volcaniclastic sites. All three sites (MY25, MY43 and MY45) record a very similar ChRM direction despite the differences in magnetic properties.

4.3.2 Sedimentary rocks

Two sites (MY24 and MY41) were established in sandstones, while two other sites (MY23 and MY42) are in limestones. In the sandstones, there is almost no unblocking of the NRM prior to 360-380°C (Fig. S8a). Above 530°C, a spurious magnetization associated with susceptibility enhancement impedes a well-defined linear demagnetization in several samples. The ChRM directions were therefore determined from data obtained over the temperature interval 320-490°C, with the best-defined lines anchored to the origin. This approach is supported by the very well-defined behaviour of some samples (sample MY2409, Fig. S8a), showing that magnetite and hematite carry the same ChRM vector.

The limestones also have a well-defined magnetization, determined mainly in the temperature range 290-530°C (Fig. S8a). The magnetization carrier is generally magnetite, but IRM acquisition data shows that 10-20% of the IRM is acquired above 250 mT. Thermal demagnetization of IRM demonstrates however that the high coercivity fraction has unblocking temperatures also between 250-330°C, while the low coercivity fraction has a more linear distribution of unblocking temperatures between 150 and 500°C.

4.3.3 Remagnetization at Kyaung Le

Despite the large differences in magnetic properties and rock types among sites, means are well-determined at eight sites and are better grouped in in-situ coordinates than after tilt correction (Fig. S8b, Supplementary Data 1), suggesting a secondary origin for the ChRM that is consistent with our petrologic observations (Supplementary section 2.3). Moreover, the volcanic sandstones and fine

breccias at site MY25 record a well-defined uniform magnetization, similar to MY43 and MY45, that is unlikely to be acquired during the formation of these rocks. $^{40}Ar/^{39}Ar$ plateau dates from MY22 and MY43 are in good agreement with those obtained for the Kanza Chaung Batholith intrusive rocks (Fig. S5). Therefore, remagnetization is likely contemporaneous with batholith emplacement.

The overall Kyaung Le in-situ mean direction shows a large clockwise rotation and a negative inclination (Supplementary Data 1). However, the in-situ means are distributed over a small circle. Sites with the steepest inclination ChRM are found in sandstones, where bedding is slightly overturned (MY24 and MY41), suggesting that some additional tilting may have occurred after remagnetization. For this reason, we consider that sites MY25, MY43 and MY45, where tilting was not large, provide the best estimate of the mean direction at Kyaung Le. The ChRM directions for these sites have shallow negative in-situ inclinations.

4.4. Kalewa (Yaw Formation)

4.4.1 Paleomagnetic directions

A total of 520 samples were collected for a magnetostratigraphic study of a ~700m thick section of the upper Eocene shallow-marine Yaw Formation in the Chindwin Basin, near Kalewa. The main magnetic mineral observed in K-T experiments (Fig. S9b) is magnetite, as shown in sandstone sample MA0275. Magnetite formation takes place in heating above 400°C in many samples containing framboidal pyrite, typically in finer-grained rocks. Greater amounts of magnetite are formed in siderite-rich samples above 450°C, hindering the identification of magnetic phases. However, IRM experiments show magnetite as the main magnetization carrier. Spurious magnetization related to magnetite formation above 400-450°C was observed in several samples, especially samples with siderite (Fig. S9a). GRM acquisition prevented further demagnetization above 400°C by AF methods. Therefore, ChRMs were mostly determined in the temperature interval ~220°C-460°C, with best-fitted lines anchored to the origin (Fig. S9a).

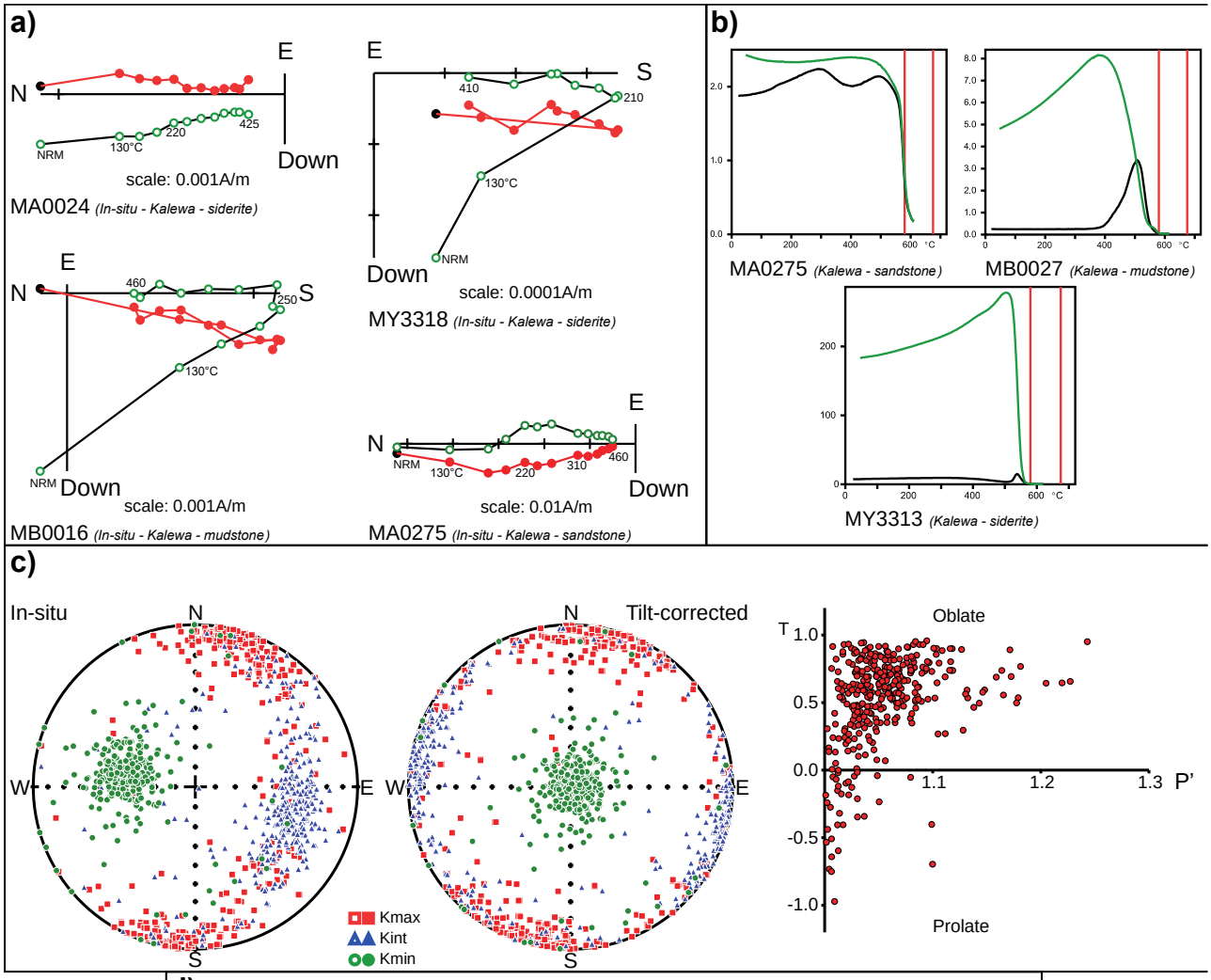
a)
N
E
Down
NRM
130°C
220
425
scale: 0.001A/m
MA0024 (In-situ - Kalewa - siderite)
S
410
210
scale: 0.0001A/m
MY3318 (In-situ - Kalewa - siderite)
460
250
MB0016 (In-situ - Kalewa - mudstone)
310
scale: 0.01A/m
MA0275 (In-situ - Kalewa - sandstone)
b)
MA0275 (Kalewa - sandstone)
MB0027 (Kalewa - mudstone)
MY3313 (Kalewa - siderite)
c)
In-situ
Tilt-corrected
W
Kmax
Kint
Kmin
Oblate
Prolate
P'
d)
In-situ
Tilt-corrected
Mean direction
Normal/reverse mean
Positive inclination
Negative inclination
Eocene APWP stable Eurasia (Torsvik et al., 2012)

Figure S9: *Paleomagnetic results from the Late Eocene Yaw Formation, Kalewa, Chindwin Basin: a) Representative orthogonal demagnetization plots from the different sampled lithologies. Open/closed dots denote projections on the vertical/horizontal plane. Reference frame, locality and lithology are indicated per plot; b) Representative bulk magnetic susceptibility (10^{-6} m^3/kg) versus temperature (°C) plots (K-T plots) up to a maximum of 590°C; c) left) Equal-area plots of the anisotropy of magnetic susceptibility (AMS) of all samples in in-situ and after bedding correction; right) plot of the shape (T) of the anisotropy ellipsoid versus the corrected degree of anisotropy (P'); d) Equal-area plots of the ChRMs of samples of the Yaw formation in both in-situ and after bedding correction.*

The most stable samples are from mudstone rocks and siderite-rich carbonate layers. In many cases, siltstones and sandstones record a significant overprint in the present-day field. These samples could be used for magnetostratigraphy, the initial goal of sampling this section, because they still yielded an indication for polarity. Unfortunately, their quality was not sufficient for calculating a mean direction. In any case, normal and reverse polarity magnetizations are present in all rock types, with well-defined polarity magnetozones. Rocks of both polarities exhibit similar magnetic behaviour during demagnetization, suggesting a detrital or early diagenetic primary origin for their remanent magnetizations. However, the resulting mean directions of the in-situ normal (N=99) and reverse (N=69) polarity groups are not perfectly antipodal: D=6.6°, I=9.1° and D = 192.2°, I=1.3°. The reversal test is negative (Fig. S10a), because the two polarity mean directions have an angular difference of 13.8°. The most likely cause is a certain degree of overprint by the present-day geomagnetic field. By iteratively subtracting an increasing percentage of this overprint direction simultaneously from both the normal and reverse mean direction, we calculated the minimum angle between the normal and reverse polarities and the possible degree of overprint. This indicates a residual overprint of about 17%. Subtracting it reduced the angular difference between the normal and reverse directions to 3.2°. Fortunately, because we have a significant number of samples of both polarities, the

magnetization overprint is cancelled out and the combined mean direction is not affected by the residual overprint.

The resulting mean is calculated with the 168 most well-defined ChRMs (99 of normal polarity and 69 of reverse polarity), showing a coherent direction with a north oriented declination and shallow inclination in tectonic coordinates (Supplementary Data 1).

4.4.2 Magnetic fabric

As defined by AMS data, the magnetic fabric of the Yaw sediments is mainly oblate and the minimum axis of the AMS fabric (Fig. S9c) is orthogonal to bedding and controlled by sedimentary processes and compaction. The exceptions to this trend are several siderite samples, which exhibit a typical inverse AMS fabric. The maximum axis is parallel to the fold axis in agreement with a tectonic imprint, typically observed in studies of rocks in orogenic belts [33]. The horizontal magnetic lineations are parallel to the axis of the Chindwin Basin. There is no local complex folding. The tectonic rotation that can be determined from our Kalewa mean direction is thus an estimate of the rotation of the whole Chindwin Basin since the late Eocene.

4.4.3. Inclination shallowing

We used two separate methods to test for inclination shallowing in the Kalewa sedimentary sequence. Our results yielded an Eocene mean inclination of 4.9±2.9° for these Eocene rocks, corresponding to a latitude of 2.4±1.5°N.

The elongation-inclination (E/I) method [34–37] gives an unflattened inclination of 7.9±4.2°, which is equivalent to a latitude of 4.0±2.1°N (Fig. S10b). The E/I method is straightforward to use, but it also has notable limitations when dealing with sedimentary sequences, because it assumes that the principal scatter in direction is caused by paleosecular variation (PSV). This is unlikely the case in slowly accumulating sedimentary deposits or when diagenetic processes average the secular variation [38]. Moreover, measurement errors, as well as the fact that normal and reverse directions

are not perfectly antipodal, can cause the data distribution to become more elongated in the horizontal plane when using the complete dataset for the E/I method.

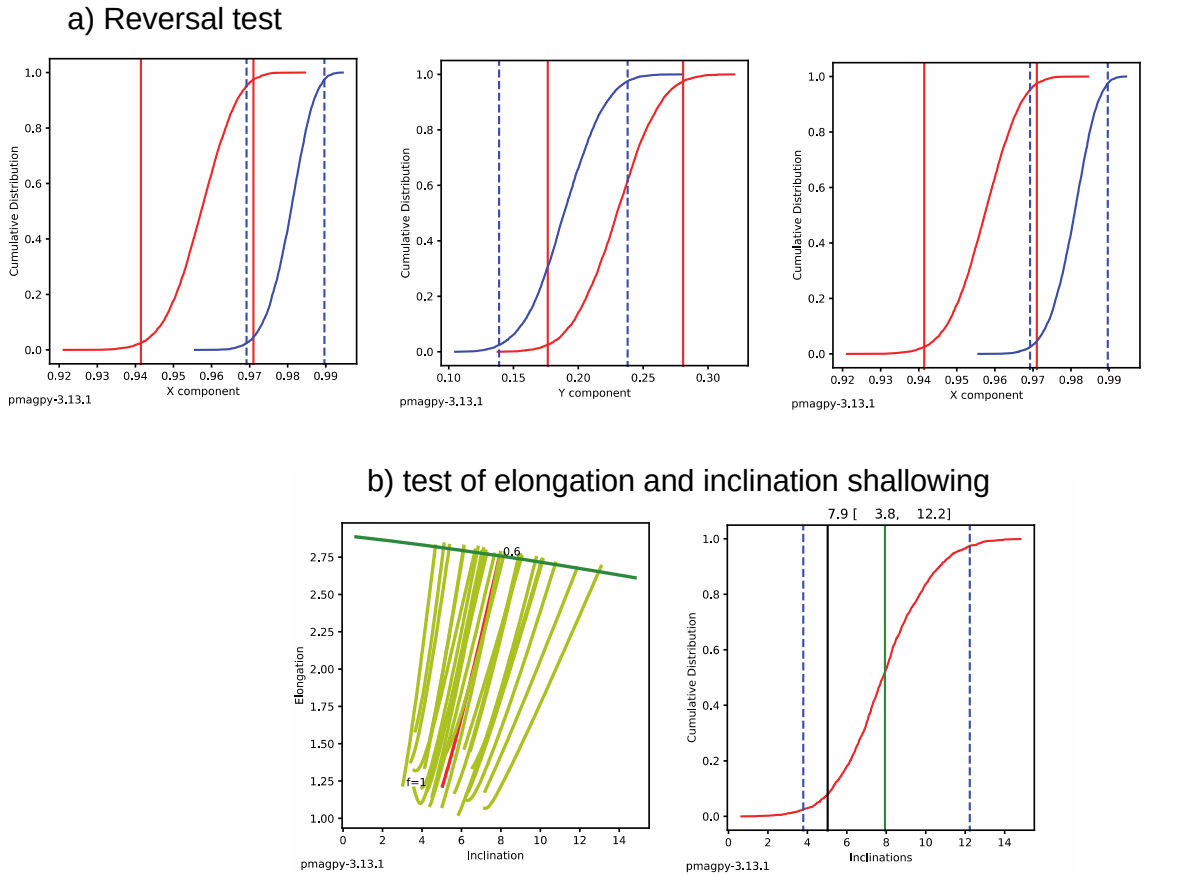

Figure S10: *a) Negative reversal test from the Kalewa sediments (Chindwin Basin) using the Cartesian coordinate bootstrap method* [54]*; b) Classic Elongation-Inclination (E-I) test to investigate the effect of inclination shallowing on the Kalewa sediments (Chindwin Basin)* [34–37]*.*

For these reasons, we opted to use a second method, with a more physical basis to test for inclination shallowing. In this second method, we assume that the sedimentary rocks consist of uniform rigid particles that rotate during coaxial shortening caused by compaction of the sediments in burial due to the overburden. Furthermore, we assume that this causes the inclination to change as a rotating passive line, resulting in the following equation [39]:

$$\tan(I_1) = \frac{\lambda_1}{\lambda_0}\tan(I_0) \qquad (1)$$

where I_1 is the measured inclination, I_0 is the unflattened inclination and $\frac{\lambda_1}{\lambda_2}$ is the strain ratio. The strain ratio is assumed to be equivalent to the ratio of initial and compacted thickness $\frac{L_1}{L_0}$ of the sedimentary package, giving:

$$\tan(I_1) = \frac{L_1}{L_0}\tan(I_0) \qquad (2)$$

The amount of shortening due to compaction is dependent on the porosity of the sediments. The relationship between change in thickness and change in porosity is given by the following relationship [40,41]:

$$\frac{L_1}{L_0} = \frac{(1-\varphi_0)}{(1-\varphi_1)} \qquad (3)$$

where ϕ_0 is the initial porosity and ϕ_1 is the final porosity. This results in the following equation:

$$\tan(I_1) = \frac{(1-\varphi_0)}{(1-\varphi_1)}\tan(I_0) \qquad (4)$$

If we now assume a total overburden of the Yaw Formation of about 2 km [28], the porosity change in an average clastic sedimentary basin should be ϕ_0=40% to a final porosity ϕ_1=27% [42]. This results in an unflattened inclination of 6.0±2.9°, equivalent to a latitude of 3.0±1.5°N.

It is possible to take into account additional physical parameters. The relationship between porosity change and compaction ΔV is given by the following equation [43]:

$$\Delta V = -\frac{(1-\varphi_0)}{(1-\varphi_1)} - 1 \qquad (5)$$

This allows us to rewrite equation (4) with ΔV = 0.18 based on our estimate of porosity change:

$$\tan(I_1) = (1 - \Delta V)\tan(I_0) \qquad (5)$$

Past laboratory compaction experiments have shown that this equation often overestimates inclination shallowing [44]. To this end, these studies added a constant factor a to equation (5), which is dependent on the shape of the magnetic particles:

$$\tan(I_1) = (1 - a\Delta V)\tan(I_0) \qquad (6)$$

If we consider the most simple assumption where the magnetizations in our sedimentary sequence are carried by equidimensional magnetite, then a = 0.54 [44]. Together with the previously determined value for ΔV = 0.18, this gives an unflattened inclination of 5.4±2.9°, equivalent to a latitude of 2.7±1.5°N. Subsequent studies [43] have determined that equation (6) approximates derivations based on different physical parameters, such as change of randomness of grain rotations and differences in initial dispersion of magnetic moments.

A final, more conservative, generalized approach is to use a ratio f=0.6 in equation (2) [45]. The corrected inclination is then 8.1±4.5° with a paleolatitude of 4.1±2.3°N.

In all cases, the influence of inclination shallowing on our results is not significant, because the initial inclination is low [34,45]. Moreover, the early-diagenetic siderite precipitated during shallow burial [31] and therefore devoid of clast reorientation during deposition and further compaction effects (See previous sections), yield inclination values equivalent to the other rock types, is another indication of negligible influence of inclination shallowing on our results.

5. Reference frame for plate reconstructions

We investigated differences in our plate tectonic reconstructions (Fig. 4) between a paleomagnetic and hotspot reference frame. At 60Ma and 95Ma there are no significant latitudinal differences between both reference frames [46]. At 40 Ma however, India and Eurasia are about 5° farther north in the paleomagnetic reference frame than in the hotspot reference frame. Indeed, low inclinations in Asia around 40 Ma have been a long-standing concern [47,48], and the global apparent polar wander path (APWP) [49] is mainly based on poles from North America (even its north-western margin with a complicated tectonic history) and north-east Africa. No pole from Siberia has been included in the calculation of the global APWP. We have recalculated the expected latitude for India using each individual pole used in the global APWP after rotation to India, using the current plate rotations from GPlates. The resulting scatter is significant and moreover the selection of several poles used in the

global APWP is questionable. In particular, two poles from late Eocene sediments and volcanics from north-east Africa are used, while they likely underwent local clockwise rotation according to the original publication [50]. Furthermore, inclination shallowing corrections were applied on results partly based on volcanic rocks [50]. Therefore, we opted to make all our plate reconstructions in the combined hotspot (0-70 Ma) and paleomagnetic (70-250 Ma) reference frame from the Matthews 2016 GPlates model [46,51], instead of a full paleomagnetic reference frame. This puts India and Eurasia slightly more to the south at that time, which also provides a better match with our 40 Ma position for the BT.

References

1. Morley, C. K. Evolution from an oblique subduction back-arc mobile belt to a highly oblique collisional margin: the Cenozoic tectonic development of Thailand and eastern Myanmar. *Geol. Soc. Lond. Spec. Publ.* **318**, 373–403 (2009).
2. Socquet, A. *et al.* India and Sunda plates motion and deformation along their boundary in Myanmar determined by GPS: GPS INDIA-SUNDA MOTION, MYANMAR STRAIN. *J. Geophys. Res. Solid Earth* **111**, n/a-n/a (2006).
3. Rangin, C., Maurin, T. & Masson, F. Combined effects of Eurasia/Sunda oblique convergence and East-Tibetan crustal flow on the active tectonics of Burma. *J. Asian Earth Sci.* **76**, 185–194 (2013).
4. Mitchell, A. H. G. Cretaceous–Cenozoic tectonic events in the western Myanmar (Burma)–Assam region. *J. Geol. Soc.* **150**, 1089–1102 (1993).
5. Metcalfe, I. Gondwana dispersion and Asian accretion: Tectonic and palaeogeographic evolution of eastern Tethys. *J. Asian Earth Sci.* **66**, 1–33 (2013).
6. Searle, M. P. *et al.* Chapter 12 Tectonic and metamorphic evolution of the Mogok Metamorphic and Jade Mines belts and ophiolitic terranes of Burma (Myanmar). *Geol. Soc. Lond. Mem.* **48**, 261–293 (2017).

7. Bertrand, G. & Rangin, C. Tectonics of the western margin of the Shan plateau (central Myanmar): implication for the India–Indochina oblique convergence since the Oligocene. *J. Asian Earth Sci.* **21**, 1139–1157 (2003).
8. Morley, C. K. Nested strike-slip duplexes, and other evidence for Late Cretaceous–Palaeogene transpressional tectonics before and during India–Eurasia collision, in Thailand, Myanmar and Malaysia. *J. Geol. Soc.* **161**, 799–812 (2004).
9. Ridd, M. F. & Watkinson, I. The Phuket-Slate Belt terrane: tectonic evolution and strike-slip emplacement of a major terrane on the Sundaland margin of Thailand and Myanmar. *Proc. Geol. Assoc.* **124**, 994–1010 (2013).
10. Rangin, C., Maurin, T. & Masson, F. Combined effects of Eurasia/Sunda oblique convergence and East-Tibetan crustal flow on the active tectonics of Burma. *J. Asian Earth Sci.* **76**, 185–194 (2013).
11. Maung, H. Transcurrent movements in the Burma–Andaman Sea region. *Geology* **15**, 911 (1987).
12. Morley, C. K. Syn-kinematic sedimentation at a releasing splay in the northern Minwun Ranges, Sagaing Fault zone, Myanmar: significance for fault timing and displacement. *Basin Res.* **29**, 684–700 (2017).
13. Morley, C. K. Chapter 4 Cenozoic rifting, passive margin development and strike-slip faulting in the Andaman Sea: a discussion of established v. new tectonic models. *Geol. Soc. Lond. Mem.* **47**, 27–50 (2017).
14. Mitchell, A., Chung, S.-L., Oo, T., Lin, T.-H. & Hung, C.-H. Zircon U–Pb ages in Myanmar: Magmatic–metamorphic events and the closure of a neo-Tethys ocean? *J. Asian Earth Sci.* **56**, 1–23 (2012).
15. Shi, G. *et al.* Ion microprobe zircon U–Pb age and geochemistry of the Myanmar jadeitite. *J. Geol. Soc.* **165**, 221–234 (2008).

16. Yui, T.-F. *et al.* Is Myanmar jadeitite of Jurassic age? A result from incompletely recrystallized inherited zircon. *Lithos* **160–161**, 268–282 (2013).

17. Barber, A. J. & Crow, M. J. Structure of Sumatra and its implications for the tectonic assembly of Southeast Asia and the destruction of Paleotethys. *Isl. Arc* **18**, 3–20 (2009).

18. Liu, C.-Z. *et al.* Tethyan suturing in Southeast Asia: Zircon U-Pb and Hf-O isotopic constraints from Myanmar ophiolites. *Geology* **44**, 311–314 (2016).

19. United Nations. Geology and exploration geochemistry of the Pinlebu-Banmauk area, Sagaing Division, northern Burma. Technical Report No. 2. DP/UN/BUR-72-002. *Geol. Surv. Explor. Proj. U. N. Dev. Programme N. Y.* 66 (1978a).

20. Sevastjanova, I. *et al.* Myanmar and Asia united, Australia left behind long ago. *Gondwana Res.* **32**, 24–40 (2016).

21. Yao, W. *et al.* Origin and tectonic evolution of upper Triassic Turbidites in the Indo-Burman ranges, West Myanmar. *Tectonophysics* **721**, 90–105 (2017).

22. Bender, F. *Geology of Burma*. (1983).

23. Pivnik, D. A. *et al.* Polyphase Deformation in a Fore-Arc/Back-Arc Basin, Salin Subbasin, Myanmar (Burma). *AAPG Bull.* **82(10)**, 1837–1856 (1998).

24. Zhang, P. *et al.* Structures, uplift, and magmatism of the Western Myanmar Arc: Constraints to mid-Cretaceous-Paleogene tectonic evolution of the western Myanmar continental margin. *Gondwana Res.* **52**, 18–38 (2017).

25. Gardiner, N. J. *et al.* Contrasting Granite Metallogeny through the Zircon Record: A Case Study from Myanmar. *Sci. Rep.* **7**, (2017).

26. Wang, J.-G., Wu, F.-Y., Tan, X.-C. & Liu, C.-Z. Magmatic evolution of the Western Myanmar Arc documented by U–Pb and Hf isotopes in detrital zircon. *Tectonophysics* **612–613**, 97–105 (2014).

27. Fareeduddin, A. & Dilek, Y. Structure and petrology of the Nagaland-Manipur Hill ophiolitic mélange zone. *NE India Foss. Tethyan Subduction Channel India-Burma Plate Bound. Episodes* **38**, 298–314 (2015).

28. Licht, A. *et al.* Paleogene evolution of the Burmese forearc basin and implications for the history of India-Asia convergence. *Geol. Soc. Am. Bull.* **1**, 20 (2018).

29. Singh, A. K. *et al.* Evidence of Mid-ocean ridge and shallow subduction forearc magmatism in the Nagaland-Manipur ophiolites, northeast India: constraints from mineralogy and geochemistry of gabbros and associated mafic dykes. *Geochemistry* **76**, 605–620 (2016).

30. Mitchell, A. *Geological Belts, Plate Boundaries, and Mineral Deposits in Myanmar*. (Elsevier, 2017).

31. Mozley, P. S. & Wersin, P. Isotopic composition of siderite as an indicator of depositional environment. *Geology* **20(9)**, 817–820 (1992).

32. Shau, Y.-H., Torii, M., Horng, C.-S. & Peacor, D. R. Subsolidus evolution and alteration of titanomagnetite in ocean ridge basalts from Deep Sea Drilling Project/Ocean Drilling Program Hole 504B9 Leg 83: Implications for the timing of magnetization. *J. Geophys. Res. Solid Earth* **105**, 23635–23649 (2000).

33. Borradaile, G. J. & Henry, B. Tectonic applications of magnetic susceptibility and its anisotropy. *Earth-Sci. Rev.* **42**, 49–93 (1997).

34. King, R. F. The remanent magnetism of artificially deposited sediments. *Geophys. J. Int.* **7**, 115–134 (1955).

35. Tauxe, L. & Kent, D. V. A simplified statistical model for the geomagnetic field and the detection of shallow bias in paleomagnetic inclinations: was the ancient magnetic field dipolar. *Timescales Paleomagn. Field* **145**, 101–116 (2004).

36. Tauxe, L., Kodama, K. P. & Kent, D. V. Testing corrections for paleomagnetic inclination error in sedimentary rocks: a comparative approach. *Phys. Earth Planet. Inter.* **169**, 152–165 (2008).

37. Koymans, M. R., Langereis, C. G., Pastor-Galán, D. & van Hinsbergen, D. J. *Paleomagnetism. org: An online multi-platform open source environment for paleomagnetic data analysis*. (Elsevier, 2016).

38. Li, Y.-X. & Kodama, K. P. Detecting and correcting for paleomagnetic inclination shallowing of sedimentary rocks: A review. *Front. Earth Sci.* **4**, 7 (2016).

39. Cogné, J.-P. Contribution a l'étude paléomagnétique des roches déformées. (Université Rennes 1, 1987).

40. Addis, M. A. & Jones, M. E. Volume changes during diagenesis. *Mar. Pet. Geol.* **2**, 241–246 (1985).

41. Brewster Baldwin. Ways of Deciphering Compacted Sediments. *SEPM J. Sediment. Res.* **Vol. 41**, (1971).

42. Ehrenberg, S. N. & Nadeau, P. H. Sandstone vs. carbonate petroleum reservoirs: A global perspective on porosity-depth and porosity-permeability relationships. *AAPG Bull.* **89**, 435–445 (2005).

43. Arason, P. & Levi, S. Models of inclination shallowing during sediment compaction. *J. Geophys. Res.* **95**, 4481 (1990).

44. Anson, G. L. & Kodama, K. P. Compaction-induced inclination shallowing of the post-depositional remanent magnetization in a synthetic sediment. *Geophys. J. R. Astron. Soc.* **88**, 673–692 (1987).

45. Tauxe, L. & Kent, D. V. Properties of a detrital remanence carried by haematite from study of modern river deposits and laboratory redeposition experiments. *Geophys. J. R. Astron. Soc.* **76**, 543–561 (1984).

46. Torsvik, T. H., Müller, R. D., Van der Voo, R., Steinberger, B. & Gaina, C. Global plate motion frames: Toward a unified model. *Rev. Geophys.* **46**, (2008).

47. Cogne, J.-P., Besse, J., Chen, Y. & Hankard, F. A new Late Cretaceous to Present APWP for Asia and its implications for paleomagnetic shallow inclinations in Central Asia and Cenozoic Eurasian plate deformation. *Geophys. J. Int.* **192**, 1000–1024 (2013).

48. Dupont-Nivet, G., van Hinsbergen, D. J. J. & Torsvik, T. H. Persistently low Asian paleolatitudes: Implications for the India-Asia collision history: PERSISTENTLY LOW ASIAN PALEOLATITUDES. *Tectonics* **29**, n/a-n/a (2010).

49. Torsvik, T. H. *et al.* Phanerozoic polar wander, palaeogeography and dynamics. *Earth-Sci. Rev.* **114**, 325–368 (2012).

50. Lofty, H. & Van der Voo, R. Tropical northeast Africa in the middle-late Eocene: Paleomagnetism of the marine-mammals site and basalts in the Fayoum province. *Egypt J Afr Earth Sci* **47**, 135–152 (2007).

51. Matthews, K. J. *et al.* Global plate boundary evolution and kinematics since the late Paleozoic. *Glob. Planet. Change* **146**, 226–250 (2016).

52. Poinar, G. Burmese amber: evidence of Gondwanan origin and Cretaceous dispersion. *Hist. Biol.* 1–6 (2018). doi:10.1080/08912963.2018.1446531

53. Grimaldi, D. A., Engel, M. S. & Nascimbene, P. C. Fossiliferous Cretaceous Amber from Myanmar (Burma): Its Rediscovery, Biotic Diversity, and Paleontological Significance. *Am. Mus. Novit.* **3361**, 1–71 (2002).

54. Tauxe, L. *Essentials of paleomagnetism*. (Univ of California Press, 2010).